Direct comparison of recombination dynamics in cubic and hexagonal GaN/AlN quantum dots

J. Simon,[1,2] N. T. Pelekanos,[2] C. Adelmann,[1] E. Martinez-Guerrero,[1] R. André,[1] B. Daudin,[1] Le Si Dang,[1] and H. Mariette[1]
[1]*CEA-CNRS Joint Group Nanophysique et Semiconducteurs, Département de Recherche Fondamentale sur la Matière Condensée, CEA Grenoble, 17 rue des Martyrs, 38054 Grenoble Cedex 9, France and Laboratoire Spectrométrie Physique (CNRS UMR5588), Université J. Fourier, Grenoble I, BP 87, 38402 Saint Martin d'Hères Cedex, France*
[2]*Microelectronics Research Group, FORTH/IESL, P.O. Box 1527, 71110 Heraklion, Greece*
(Received 9 July 2002; revised manuscript received 28 January 2003; published 14 July 2003)

We report on time-integrated and -resolved photoluminescence (PL) data on self-assembled GaN quantum dots (QD's) embedded in AlN, in both cubic [zinc-blende (ZB)] and hexagonal [wurtzite (Wz)] crystallographic phases. The comparison of the optical properties of ZB and Wz nitride QD's allows us to distinguish pure dimensionality effects from the influence of the large polarization-induced electric fields present in the Wz nanostructures. Specifically, the PL energy of the ZB QD's is always higher than the bulk cubic GaN band-gap energy, in contrast to the Wz QD's where a 7-MV/cm polarization field gives rise to below-gap PL emission for sufficiently large QD's. As a further consequence of the internal field, the low-temperature PL decay times of the Wz QD's are significantly longer than the ZB ones, and increase strongly with the QD height in contrast to the ZB ones, which exhibit only a small size dependence. For both types of QD's, the PL intensity is found to be weakly dependent on temperature, underscoring the strong zero-dimensional exciton localization in the GaN/AlN system. In spite of the strong localization, however, we show that the nonradiative channels cannot be neglected and have a significant contribution in the PL decay time for both ZB and Wz QD's.

DOI: 10.1103/PhysRevB.68.035312 PACS number(s): 78.67.Hc, 78.55.Cr, 78.47.+p

I. INTRODUCTION

Wurtzite (Wz) InGaN/GaN quantum wells (QW's) have been extensively studied for their use in blue and green light-emitting devices.[1,2] More recently, a lot of effort has been dedicated also to the optical study of Wz GaN/AlGaN QW's. Aside from their potential use in UV laser diodes, the GaN/AlGaN system is, in principle, well suited to investigate the generic optical properties of nitride QW's, since the wells consist of a binary compound and are free of the local composition fluctuations present in InGaN QW's. However, it was found that two effects dominate the recombination dynamics of Wz GaN/AlGaN QW's and raise serious difficulties for understanding their properties. The first one is the presence of very large polarization-induced electric fields,[3–8] of the order of MV/cm, perpendicular to the QW plane. Such fields separate spatially the electrons and holes leading to reduced wave-function overlap and increased radiative recombination times. As an example, in a $GaN/Al_{0.24}Ga_{0.76}N$ heterostructure the polarization field was found to be as high as 1.3 MV/cm,[8] a value which cannot be ascribed merely to piezoelectric effects, but rather is the outcome of the combined action of piezoelectric and spontaneous polarizations in the structure. The second limiting effect is the varying from sample-to-sample degree of in-plane exciton localization due to QW width and polarization field fluctuations, which can overshadow the intrinsic effects that govern the recombination dynamics in GaN QW's.

In this work, we compare systematically the photoluminescence (PL) and time-resolved photoluminescence (TRPL) properties of cubic [zinc-blende (ZB)] and hexagonal (Wz) GaN/AlN quantum dots (QD's). Studying QD's instead of QW's allows us to deal at all temperatures with strongly localized excitons, rather than a thermodynamic balance between free and localized excitons in the QW case. Furthermore, comparing the optical properties of ZB and Wz QD's allows the deconvolution of pure dimensionality effects from the influence of the giant 7-MV/cm polarization field present in the Wz QD's.[9] The paper is organized as follows: the samples and the experimental setup are described in Sec. II. The PL results on several ZB and Wz GaN/AlN QD samples are discussed in Sec. III. In Sec. IV, we report and compare the low-temperature TRPL results obtained on Wz and ZB GaN/AlN QD's. The dynamic behavior as a function of temperature is presented for both phases in Sec. V. A summary of the main results and conclusions is reported in Sec. VI.

II. SAMPLES AND EXPERIMENT

It is well known that even though nitrides are grown naturally in the Wz phase, under certain conditions, they can be induced to grow also in the ZB phase.[10] The QD samples discussed here are multiple period self-assembled GaN QD's on AlN, grown by molecular-beam epitaxy on (100)SiC/Si substrates for the ZB phase and on *c*-axis GaN/Al_2O_3 for the Wz one. The growth was monitored *in situ* using reflection high-energy electron diffraction, which allows to control either the formation of two-dimensional layers or the Stranski-Krastanow transition for the formation of QD's. The metal fluxes were provided by standard effusion cells, while active nitrogen was derived from the radio-frequency dissociation of N_2 using a plasma cell. The samples were grown at 700 °C and at stochiometry conditions proper to induce the Stranski-Krastanow transition.[9] The QD's studied here have a typical height of 30 Å with a diameter-to-height aspect ratio of 5 in the Wz case,[11] and of 10 in the ZB case.[12] The QD density is a few times 10^{11} cm^{-2}.[13] More specifically, the two samples studied in detail in TRPL spectroscopy have the following characteristics: the Wz sample consists of 72 periods of GaN QD's separated by 100-Å-thick AlN spacer layers, grown on

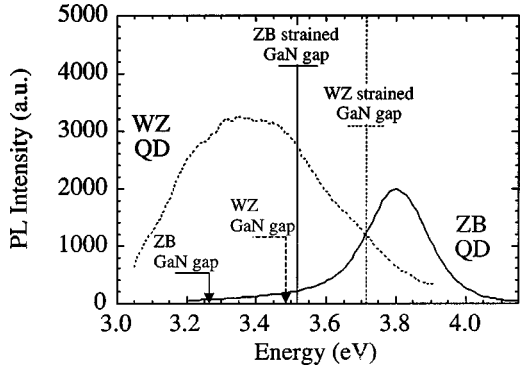

FIG. 1. PL spectra at $T=10$ K of ZB (solid curve) and Wz (dashed curve) GaN/AlN QD's. The respective unstrained and strained band gaps for GaN in each phase are indicated for comparison (solid and dashed lines).

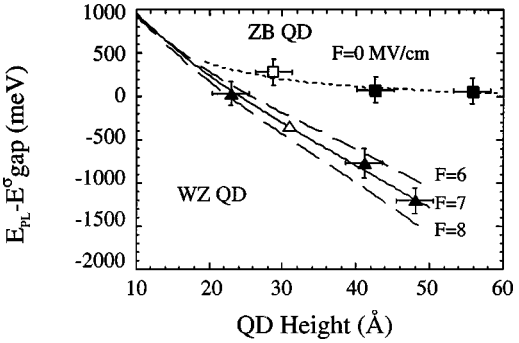

FIG. 2. Energy shift of QD PL with respect to the GaN strained band gap as a function of QD height for ZB (squares) and Wz (triangles) QD samples of different QD heights. The open symbols indicate the samples studied in detail in this work. The error bars correspond to the width of the QD-height distribution for the *x* axis and the PL full width at half maximum for the *y* axis. The curves are calculated estimates as a function of internal electric field.

a 0.5-μm-thick AlN buffer layer deposited directly on a sapphire substrate. The ZB sample was grown on a 3C-SiC/Si pseudosubstrate, covered by a 500-Å AlN buffer layer, and followed by ten periods of GaN QD's separated by 100-Å-thick AlN layers.

The TRPL experiments were performed in a standard streak camera setup having an instrument response of 2 ps, and the excitation source was 1-ps pulses with a 76-MHz repetition rate of a frequency-tripled Ti-sapphire laser with $\lambda_x=266$ nm. Using this setup we were able to extract long decay times (2–10 ns) by fitting the acquired decay curves, taking into account corrections related to contributions to the streak signal from more than one linear region of the sinusoidal high voltage. The average power density of excitation was 10 W/cm^2, for which the generated per pulse exciton density is two orders-of-magnitude below the QD density, therefore, we can safely assume in our analysis that we are dealing with single-exciton recombination and that screening effects in the Wz QD's are negligible. It should be noted that the energy of excitation ($E_x=4.67$ eV) is below the AlN energy gap and, hence, the GaN QD's were pumped by direct absorption in the QD excited states.

III. PHOTOLUMINESCENCE EXPERIMENTS

In Fig. 1, typical $T=10$-K time-integrated PL spectra are shown for both the Wz and ZB QD samples. As argued in Ref. 9, the PL spectra are due to intrinsic emission from the QD ground states. The relative positions of the two PL peaks contain important information. The PL peak of the ZB QD is centered at 3.8 eV, i.e., 0.3 eV *above* the strained cubic GaN energy gap. In the latter, we have included an estimated strain-induced blueshift of the gap of $\sim$0.25 eV due to the 2.5% biaxial compression present in the GaN QD's. For this estimate we have used Wz coefficients.[14] On the other hand, the Wz QD PL peak is centered at $\approx$3.3 eV, i.e., 0.4-eV *below* the Wz GaN gap under strain.[14] Let us note that the strain GaN gap energy position reported in Fig. 1, for both crystallographic phases, has been estimated assuming an uniform strain throughout the dot. However, the uncertainties related to this assumption are less important than the one related to the GaN parameters (hole effective mass, valence-band offset, deformation potential). Moreover, such a hypothesis does not affect the value found for the electric field present in the Wz structures, since this value depends only on the relative energy variation of the excitonic emission as a function of QD height (see Fig. 2). Then the energy shift between the two emission bands in Wz and ZB GaN dots is a clear manifestation of the polarization field present in the Wz QD's, which redshifts the intrinsic QD transitions by the quantum-confined Stark effect. The large PL linewidth in the Wz case is also a side effect of the internal field, which amplifies the PL line broadening by QD size fluctuations. The PL spectra of Fig. 1 were obtained under identical excitation conditions, in order to be able to compare the spectrally integrated PL intensities of the two samples in an absolute manner, a point that will prove very useful in the discussion of the recombination dynamics of Sec. IV.

The relative shift of the QD PL energy with respect to the GaN strained band gap is reported in Fig. 2 for several ZB and Wz QD samples of different QD heights. As described elsewhere,[13] it is possible to vary the QD size in both phases by employing a ripening stage during the growth of the QD's. The QD height is determined by atomic force or transmission-electron microscopy (TEM).[9,11–13] We observed a dramatic dependence of the Wz QD PL emission energy on the QD size,[9] compared to the smooth variation in the ZB case. Note, in particular, that 56-Å-high ZB QD's still emit above the ZB GaN strained band gap. In order to estimate the electric field present in the Wz QD's, we compare the experimental results with calculations of the QD ground-state transition energy as a function of the QD size for various input values of the electric field (for details of the calculation see Ref. 9). The variation of the exciton binding energy with the electric field and the QD size have been taken into account for the calculated curves. As can be seen in Fig. 2, by assuming an internal electric field of 7 MV/cm we can reproduce well the experimental points of Wz QD's. The strength of the field is in accordance with the giant piezoelectric and spontaneous polarizations expected to be present in Wz nitrides.[15,8] On the other hand, the zero-field curve correctly predicts the ZB QD emission energies, con-

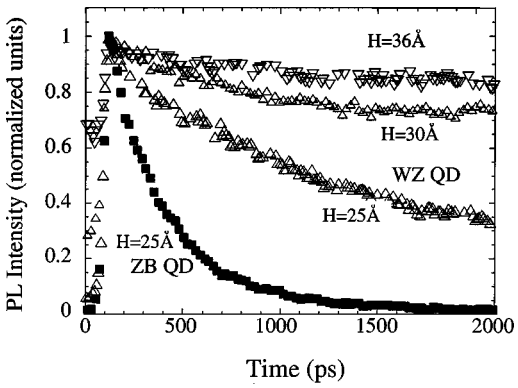

FIG. 3. PL decay curves of Wz QD's (open triangles) of various QD heights 36, 30, and 25 Å, corresponding to the low-, intermediate-, and high-energy sides of the Wz PL peak in Fig. 1. The QD heights are deduced according to Fig. 2. For comparison the PL decay curve of ZB QD's with $H=25$ Å is also plotted (solid squares).

firming the absence of any internal field in the ZB QD's in agreement with symmetry arguments. Knowing from Fig. 2 the exact dependence of the PL emission energy on the QD height for both phases, we can associate every spectral component of the PL spectra of Fig. 1 with a corresponding QD height.

IV. LOW-TEMPERATURE TRPL EXPERIMENTS

In Fig. 3, we show the PL decay curves (open symbols) from three different spectral windows of the Wz QD PL shown in Fig. 1, corresponding to QD heights of 25, 30, and 36 Å according to Fig. 2. For comparison, the PL decay curve (solid squares) for 25-Å-high ZB QD's is also plotted, exhibiting a much faster decay compared to the Wz QD's. All decay curves can be fitted by single exponentials, in agreement with the absence of screening effects. As the Wz QD height increases from 25 to 36 Å the PL decay time τ_D varies from 1.8 to 7.5 ns, indicating a pronounced size dependence for the Wz QD's, which is plotted in Fig. 4(a). By contrast, no such dependence is observed in Fig. 4(b) for the ZB QD's.

For the Wz structures, the variation of τ_D with the QD height is consistent with the larger field-induced electron-hole separation in the larger QD's. Nevertheless, we observe in Fig. 4(a) that τ_D saturates for QD heights larger than 34 Å. We interpret this saturation as an indication that for $H>34$ Å τ_D is dominated by nonradiative processes even at $T=10$ K.

The measured PL decay time τ_D of a QD with height H at temperature T is related to the radiative and nonradiative recombination times τ_R and τ_{NR}, respectively, by

$$\frac{1}{\tau_D(H,T)}=\frac{1}{\tau_R(H,T)}+\frac{1}{\tau_{NR}(H,T)}. \tag{1}$$

The internal radiative efficiency of a QD of height H, $\eta(H,T)$, is then defined as

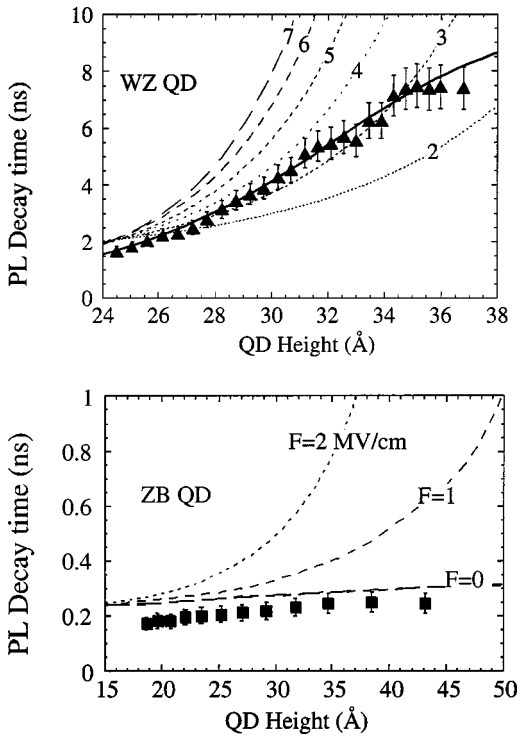

FIG. 4. (a) Comparison for the Wz QD's of experimental decay times $\tau_D(H)$ (solid triangles) with theoretical radiative times $\tau_R(H,F)$ (dashed curves) calculated for various internal electric fields F (in units of MV/cm) and the hypothesis $\eta_{SD}=0.8$. The solid line running through the data points is the theoretical $\tau_D(H)$ curve obtained assuming $F=7$ MV/cm and $\tau_{NR}=10$ ns (b) Comparison for the ZB QD's of experimental $\tau_D(H)$ (solid squares) with theoretical $\tau_R(H,F)$ times (dashed lines) for various electric fields and assuming $\eta(30\text{ Å})=0.787$.

$$\eta(H,T)=\frac{\tau_{NR}(H,T)}{\tau_{NR}(H,T)+\tau_R(H,T)}=\tau_D(H,T)/\tau_R(H,T). \tag{2}$$

In order to analyze τ_D in terms of radiative and nonradiative contributions, an assumption is needed at this stage for $\eta(H,10\text{ K})$.[16] The usual assumption employed for QW's (Refs. 6 and 17) is that the low temperature τ_D is purely radiative, i.e., $\eta(H,10\text{ K})=1$. Obviously, however, this assumption is not applicable in our case of Wz QD's, since it would be impossible to explain the observed saturation of τ_D for $H>34$ Å.

Instead of making an assumption on $\eta(H,10\text{ K})$ for every H, the problem can be reduced to a unique assumption on the radiative efficiency of the smaller dots (SD), η_{SD}, with $H_{SD}=25$ Å by calculating theoretically the oscillator strength f ($\sim 1/\tau_R$) as a function of H, with an electric field of 7 MV/cm present in the QD confinement potential (for details of the calculation see Ref. 7). Fixing η_{SD} is then equivalent to fixing the proportionality coefficient between τ_R and $1/f$. Knowing then $f(H)$, we can obtain $\tau_R(H)$ and, through Eq. (1), $\tau_{NR}(H)$. Note that the τ_R dependence on H and T does not change with η_{SD} within a multiplication factor,[16] whereas $\tau_{NR}(H,T)$ is very sensitive to the chosen value of η_{SD}. This can be seen in Fig. 5, where we plot

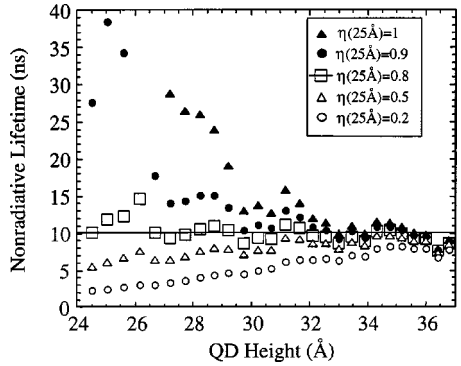

FIG. 5. Nonradiative recombination time τ_{NR} in Wz QD's as a function of QD height H, assuming $F=7$ MV/cm and various values of $\eta(25\ \text{Å})$. For $\eta(25\ \text{Å})>0.8$ (solid symbols) τ_{NR} decreases with H, while for $\eta(25\ \text{Å})<0.8$ (open symbols) it increases. Large open squares represent the $\eta(25\text{-Å})=0.8$ case, adopted in our analysis, for which we have a constant τ_{NR}.

$\tau_{NR}(H)$ for different values of η_{SD} and $F=7$ MV/cm: τ_{NR} is found to decrease with H when $\eta_{SD}>0.8$, and to increase when $\eta_{SD}<0.8$. A TEM study has shown that the Wz QD's, though free of misfit dislocations, nucleate next to threading edge dislocations of the AlN matrix,[18] which may be one of the main sources of nonradiative recombination. Smaller QD's are expected to have larger wave-function penetration in the AlN and therefore shorter τ_{NR}. Hence, we conclude from Fig. 5 that $\eta_{SD}\cdot 0.8$. On the other hand, this size dependence of τ_{NR} should be rather moderate based on the fact that due to the very large internal field in the QD's the carriers are squeezed at the opposite GaN/AlN heterointerfaces,[19] where they face approximately the same triangular potential in this QD-height range with no significant variation in the wave-function tail. In what follows, we assume that $\eta_{SD}=0.8$, which corresponds to the simplest situation for which τ_{NR} is independent of H and equal to $\sim$10 ns. This assumption allows us to analyze the experimental τ_D as a function of QD height [Fig. 4(a)].

The dashed lines in Fig. 4(a) represent τ_R obtained from calculations of f for various values of electric field with the assumption $\eta_{SD}=0.8$. First of all, we note that the τ_R curves fail to reproduce the experimental τ_D, whatever the field value in the GaN QD, which confirms the contribution of nonradiative channels even at low temperature. On the other hand, the solid curve running through the experimental τ_D points is obtained by Eq. (1) assuming $\tau_{NR}=10$ ns is independent of H, and $\tau_R(H)$ is the dashed curve corresponding to a 7-MV/cm field in the QD, in agreement with the conclusions of Fig. 2. Clearly, the solid curve reproduces well the experimental points, including the saturation of τ_D for the larger dots. In Fig. 6(a) we plot for the Wz QD's (triangles) $\eta(H,10\ \text{K})$ as a function of H, deduced by dividing the experimental $\tau_D(H)$ by the $\tau_R(H)$ curve for 7 MV/cm. We observe a drastic reduction of η from 0.8 for the smaller dots ($H=25$ Å) to 0.25 for the larger ones ($H=36$ Å). This strong decrease reflects the strong reduction of oscillator strength due to the electric field.

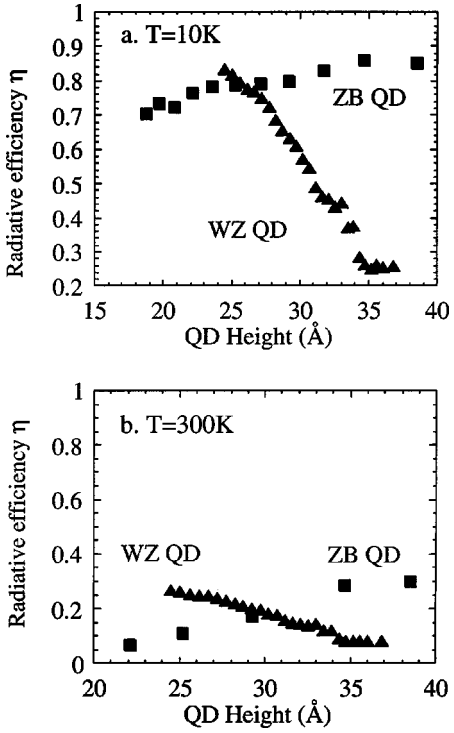

FIG. 6. Comparison of radiative efficiency η as a function of QD height for Wz and ZB QD's at (a) $T=10$ and (b) 300 K. Note the significantly larger η achieved by the ZB QD's, in spite of the much shorter nonradiative times.

In order to compare on an absolute scale the decay times of the ZB QD's with the Wz ones, we need to somehow relate the radiative efficiency of the ZB QD's with that of the Wz QD's. This is possible by comparing the spectrally integrated PL intensity, I_{PL}, for the two samples in Fig. 1, since I_{PL} can be written as

$$I_{PL}=I_0\,.\,\overline{\eta}, \tag{3}$$

where I_0 is a normalization factor depending on the number of photoexcited carriers and $\overline{\eta}$ the spectrally averaged radiative efficiency. From Fig. 6(a) we deduce that $\overline{\eta}\cdot 0.53$ for the Wz QD's, which corresponds approximately to η at the center of the QD distribution ($H=30$ Å). In order to compare the I_{PL} from Fig. 1, we normalize the I_{PL} of the Wz QD sample with 72 QD planes to that of the ZB QD sample with 10 QD planes, by considering the absorption of the excitation beam ($\lambda_{exc}=266$ nm) by each QD layer. We determined experimentally that each QD layer absorbs 0.7% of the incident beam at $\lambda=266$ nm, which allows us to determine the correction factor. Then by comparing the I_{PL} of the two samples, we deduce that $\overline{\eta}_{ZB}=0.787$.

Considering the small size dependence of τ_D in the ZB QD's, it is reasonable to expect a similar small dependence of η on H. Henceforth, we assume that $\overline{\eta}_{ZB}=\eta(H=30\ \text{Å})=0.787$, i.e., at the center of the ZB QD distribution. In Fig. 4(b) we compare for the ZB QD's the experimental $\tau_D(H)$ points with the theoretical $\tau_R(H,F)$ times (dashed lines), obtained for various electric fields and assuming $\eta(30\ \text{Å})$

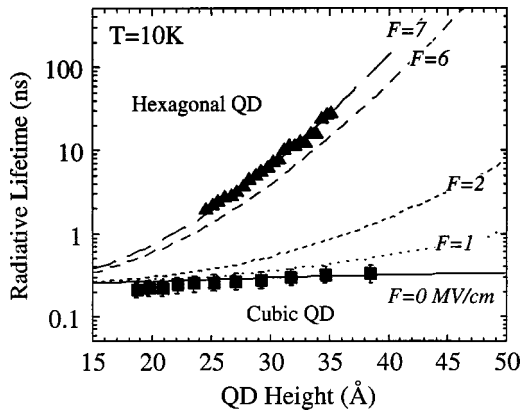

FIG. 7. Absolute comparison of experimental radiative recombination times $\tau_R(H)=\tau_D(H)/\eta(H)$ with inverse oscillator strength α/f curves for various electric fields. The proportionality coefficient α is fixed such that $\eta_{SD}(25\ \text{Å})=0.8$ for the Wz QD's and is kept constant for all α/f curves. Note the very good agreement between the ZB-$\tau_R(H)$ and $F=0$-α/f curve (solid line). Vertical error bars on the ZB QD's represent an uncertainty of 20% concerning the absorption coefficient in ZB QD's.

$=0.787$. Clearly, only the zero-field curve can reproduce the small size dependence of τ_D for the ZB QD's, as expected.

Knowing τ_D and τ_R we can deduce τ_{NR}, which is found to be ·0.8 ns for the ZB QD's and almost independent of H. Its absolute value is about ten times lower than the one inferred for the Wz QD's. This difference in τ_{NR} between the two types of QD's can be attributed to the larger density of defects in the ZB samples (see below). Finally, we determine $\eta(H,10\ \text{K})$ for the ZB QD's, which is reported in Fig. 6(a). Contrary to Wz QD's, η_{ZB} increases with H from 0.7 to 0.86 as H varies from 20 to 35 Å. Such a different behavior can be accounted for by the absence of any polarization field in the case of ZB QD's.

Figure 7 presents the comparison on an absolute scale between the experimental and the calculated values of τ_R in Wz and ZB QD's as a function of H. The experimental τ_R are obtained from the experimental τ_D values of Fig. 4, by applying Eq. (2) and using Fig. 6(a). The calculated curves of τ_R correspond to α/f curves estimated for different electric fields, where α is the proportionality coefficient deduced from the assumption $\eta_{SD}(25\ \text{Å})=0.8$ for the Wz QD's. Then, as shown in Fig. 7, the agreement for both phases between experimental τ_R points and theoretical α/f curves is excellent, assuming that the Wz QD's contain an internal field of 7 MV/cm, whereas for the ZB QD's there is no internal field. The good agreement demonstrates that the oscillator strength in the ZB nanostructures remains basically unaffected by the QD height in the range (20–40 Å), and that τ_R is about of 200–300 ps whereas the Wz QD's show instead a strong size dependence with the τ_R ranging from a few ns to a few tens of ns for QD heights in the range 25–35 Å.

V. TEMPERATURE-DEPENDENT TRPL EXPERIMENTS

Based on combined measurements of τ_D and I_{PL} as a function of temperature, we can extract both $\tau_R(T)$ and

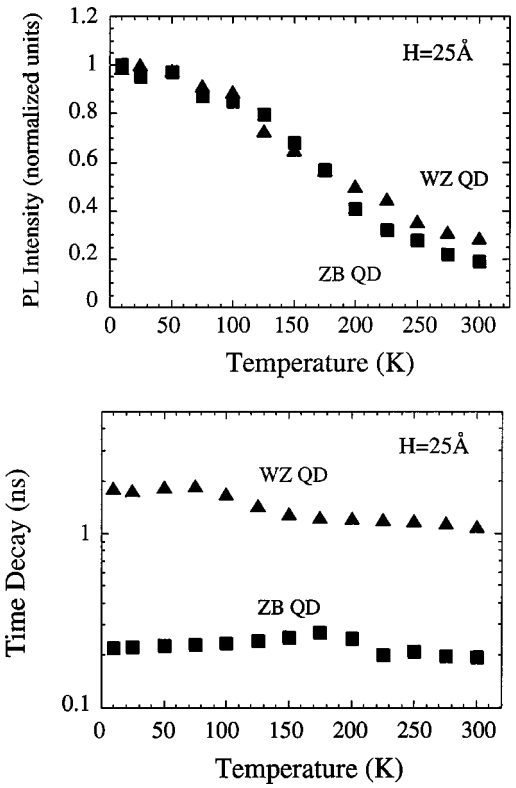

FIG. 8. Integrated PL intensity (a) and PL decay time (b) versus temperature for Wz (triangles) and ZB (squares) QD's with $H=25$ Å.

$\tau_{NR}(T)$ from Eqs. (1) and (3) as follows:

$$\tau_R(H,T)=I_0\cdot\frac{\tau_D(H,T)}{I_{PL}(H,T)}=\frac{\tau_D(H,T)}{\eta(H,T)}, \tag{4}$$

$$\tau_{NR}(H,T)=\tau_D(H,T)\cdot\frac{I_0}{I_0-I_{PL}(H,T)}=\frac{\tau_D(H,T)}{1-\eta(H,T)}. \tag{5}$$

The temperature dependence of the PL intensity for 25-Å-high Wz and ZB QD's is reported in Fig. 8(a). We observe a very similar decrease of the QD PL intensity by less than one decade between low and high temperatures for both types of QD's. The small decrease contrasts with GaN/AlGaN QW samples, which always show a decrease of several orders of magnitude in this range of temperatures.[20] This is coherent with the stronger localization of carriers in the QD's, which hinders thermal escape and effectively protects the carriers from thermally activated nonradiative channels. On the other hand, the very similar variation for the two types of QD's is quite surprising, considering the large difference between τ_R (cf. Fig. 7), which should have led to enhanced radiative efficiencies for the ZB QD's. It can be understood, however, by the much shorter τ_{NR} times in the ZB QD's (·0.8 ns) compared to the ones in Wz QD's (·10 nsec).

In Fig. 8(b) we plot the experimental τ_D values versus temperature for 25-Å-high ZB and Wz QD's. In contrast to QW's or quantum wires, where the density of states permits thermalization of the carriers inducing an increase of τ_R with

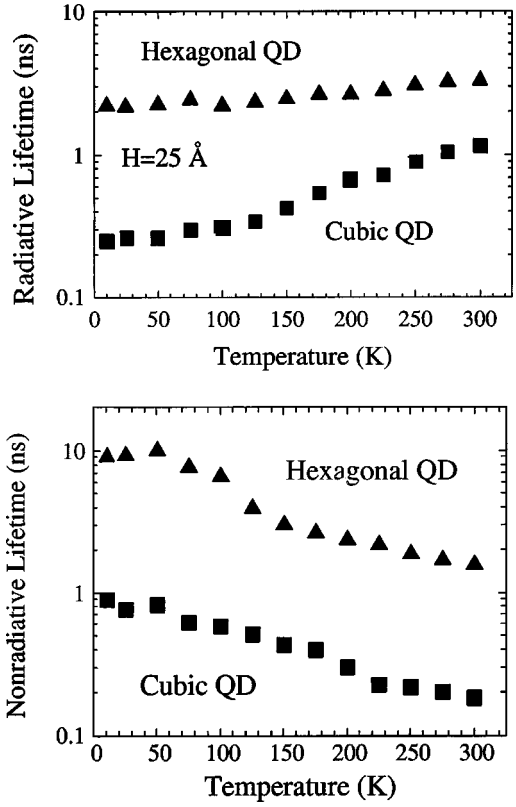

FIG. 9. Radiative (a) and nonradiative (b) recombination times versus temperature for Wz (triangles) and ZB (squares) QD's with $H=25$ Å. Note the stronger increase of τ_R for the ZB QD's, and that τ_{NR} is at all temperatures one order-of-magnitude shorter in the ZB QD sample.

temperature,[21–24] the discrete density of states in the case of QD's forbids any temperature-induced variation of the oscillator strength.[25] Hence, provided that radiative processes dominate in the PL decay, we do not expect any significant temperature variation of τ_D in our QD's, in qualitative agreement with Fig. 3(b).

In Figs. 9(a) and 9(b), we plot the temperature dependence of τ_R and τ_{NR}, respectively, for 25-Å-high Wz and ZB QD's. τ_R and τ_{NR} are deduced from the experimental data using Eqs. (4) and (5). We observe that for the Wz QD's τ_R remains relatively constant in the whole temperature range, manifesting the zero-dimensional character of the system. Contrarily, the ZB QD's exhibit a significant increase of τ_R with temperature, suggesting that the dimensionality of the system is somewhere between zero and two dimensional. This different behavior can be associated with the larger diameter-to-height ratio for the ZB QD's. At room temperature, in spite of the faster τ_R increase for the ZB QD's, still the Wz QD's exhibit longer τ_R. This τ_R difference is compensated by a similar ratio between the room temperature τ_{NR} for the two types of QD's. The variation of τ_{NR} with temperature is similar in both phases as shown in Fig. 9(b). A TEM study has shown that a large number of stacking faults are present along {111} planes in the cubic phase.[12] Even if islands grow preferentially within each domain bounded by these stacking faults, we expect that the numerous defects play a significant role on the short τ_{NR} times.

A more detailed study of τ_{NR} times in the Wz QD's tends indeed to show that the threading dislocations present near the edge of the Wz dots[18] participate in the nonradiative processes at higher temperatures. While, at low temperature, the emission dynamics of the Wz QD's are described by a unique τ_{NR} for all H, at room temperature we observe an increase of τ_{NR} with increasing H. Thus, for QD's with $H=36$ Å $\tau_{NR}=3.5$ ns at 300 K, whereas for $H=25$ Å $\tau_{NR}=1.2$ ns. This shows that the smaller dots are more sensitive to nearby defects, which is coherent with the carrier wavefunction extending more outside the QD's.

We would like now to discuss in more detail the temperature dependence of τ_R in our QD's. For the Wz QD's, τ_R remains constant up to 130 K and then increases slightly by a factor of 1.6 between 150 and 300 K. This behavior could be attributed to some carrier thermalization between the ground and first excited states in the QD. The fact that τ_R increases above 150 K (corresponding to $\cdot E \approx 15$ meV) gives a rough estimate of the energy separation between the two states. This value is coherent with the energy of the first excited states resulting from lateral confinement in the plane, considering that the QD diameter is between 100 and 200 Å. Their growing contribution with temperature may thus lead to increased τ_R. This picture can also explain the experimental results on the ZB QD's, where τ_R remains constant up to 50 K and increases by a factor of 5 between 50 K and room temperature [Fig. 9(a)]. Considering that the ZB QD's have a diameter-to-height ratio of 10 instead of 5 in the Wz QD's, the excited states are then closer to each other and the effect on τ_R by thermalization is more efficient, even at temperatures as low as 50 K.

Finally, the room-temperature internal radiative efficiency η as a function of QD height is reported in Fig. 6(b). For the Wz QD's, η is maximum for the smallest QD's with $\eta(H=25\text{ Å})=0.27$. When the QD size increases, η decreases mainly due to the strong increase of τ_R (see Fig. 7). Nevertheless, the decrease is considerably weaker than considering τ_R alone, because of the parallel increase with the QD size of *both* τ_R and τ_{NR} at room temperature. This is a crucial point for understanding the way in which these hexagonal nanostructures are very attractive for their optical efficiency, in spite of their longer τ_R. As for the ZB QD's, in contrast to the Wz case, η is maximal for larger dots with η varying from 0.05 to 0.3 for $H=20-37$ Å. Note that for $H>30$ Å, the room temperature η reaches higher values in the cubic phase, despite limited crystalline quality.

VI. CONCLUSIONS

Time-integrated and -resolved PL spectroscopy has been used to study cubic and hexagonal GaN nanostructures. Our results revealed the important role played by the exciton localization and polarization fields in the recombination dynamics of nitride nanostructures. Specifically, we demonstrated that the radiative lifetime in hexagonal QD's is more than one order-of-magnitude longer than in comparable

cubic QD's, a fact unambiguously related to the presence of the internal polarization fields in hexagonal QD's. Furthermore, we observed a strong size dependence of the radiative decay times in the hexagonal QD's, also as a consequence of the strong polarization field. We showed that nonradiative processes should be taken into account even at low temperatures ($T = 10$ K), and that in hexagonal QD's they are at least one order-of-magnitude less efficient than in cubic QD's due to superior crystalline quality. In spite of this, we found comparable radiative efficiencies in the two types of QD's, mainly because of the much faster radiative times in the cubic phase.

[1] S. Nakamura, M. Senoh, S.-I. Nagahama, N. Isawa, T. Yamada, T. Matsuhita, Y. Sugimoto, and H. Kiyoku, Jpn. J. Appl. Phys., Part 2 **36**, L1059 (1997).

[2] S. Nakamura, M. Senoh, N. Isawa, and S.-I. Nagahama, Appl. Phys. Lett. **67**, 1868 (1996).

[3] M. Smith, J. Y. Lin, H. X. Jiang, A. Salvador, A. Botchkarev, W. Kim, and H. Morkoç, Appl. Phys. Lett. **69**, 2453 (1996).

[4] J. S. Im, H. Kollmer, J. Off, A. Sohmer, F. Scholz, and A. Hangleiter, Phys. Rev. B **57**, R9435 (1998).

[5] M. Leroux, N. Grandjean, M. Laügt, J. Massies, B. Gil, P. Lefevre, and P. Bigenwald, Phys. Rev. B **58**, R13 371 (1998).

[6] P. Lefebvre, J. Allègre, B. Gil, H. Mathieu, N. Grandjean, M. Leroux, J. Massies, and P. Bigenwald, Phys. Rev. B **59**, 15 363 (1999).

[7] R. Langer, J. Simon, V. Ortiz, N. T. Pelekanos, A. Barski, R. André, and M. Godlewski, Appl. Phys. Lett. **74**, 3827 (1999); R. André, J. Cibert, and Le Si Dang, Phys. Rev. B **52**, 12 013 (1995).

[8] J. Simon, R. Langer, A. Barski, and N. T. Pelekanos, Phys. Rev. B **61**, 7211 (2000); J. Simon, R. Langer, A. Barski, M. Zervos, and N. T. Pelekanos, Phys. Status Solidi A **188**, 867 (2001).

[9] F. Widmann, J. Simon, B. Daudin, G. Feuillet, J. L. Rouviere, N. T. Pelekanos, and G. Fishman, Phys. Rev. B **58**, R15 989 (1998).

[10] For a review, see, for instance, O. Brand, in *Group III Nitride Semiconductor Compounds* (Clarendon, Oxford, 1998).

[11] C. Adelmann, J. Brault, J.-L. Rouvière, H. Mariette, G. Mula, and B. Daudin, J. Appl. Phys. **91**, 5498 (2002).

[12] E. Martinez-Guerrero, C. Adelmann, F. Chabuel, J. Simon, N. T. Pelekanos, G. Mula, B. Daudin, G. Feuillet, and H. Mariette, Appl. Phys. Lett. **77**, 809 (2000).

[13] B. Daudin, G. Feuillet, H. Mariette, G. Mula, N. T. Pelekanos, E. Molva, J. L. Rouvière, C. Adelmann, E. Martinez-Guerrero, J. Barjon, F. Chabuel, B. Bataillou, and J. Simon, Jpn. J. Appl. Phys., Part 1 **40**, 1892 (2001).

[14] B. Gil, O. Briot, and R. L. Aulombard, Phys. Rev. B **52**, R17 028 (1995).

[15] F. Bernardini, V. Fiorentini, and D. Vanderbilt, Phys. Rev. B **56**, R10 024 (1997).

[16] M. Gurioli, A. Vinattieri, M. Colocci, C. Deparis, J. Massies, G. Neu, A. Bosacchi, and S. Franchi, Phys. Rev. B **44**, 3115 (1991).

[17] P. Lefebvre, J. Allegre, B. Gil, A. Kavokin, H. Mathieu, W. Kim, A. Salvador, A. Botchkarev, and H. Morkoc, Phys. Rev. B **57**, R9447 (1998).

[18] J. L. Rouviere, J. Simon, N. T. Pelekanos, B. Daudin, and G. Feuillet, Appl. Phys. Lett. **75**, 2632 (1999).

[19] A. D. Andreev and E. P. O'Reilly, Phys. Rev. B **62**, 15 851 (2000).

[20] J. Simon, E. Martinez-Guerrero, C. Adelmann, G. Mula, B. Daudin, G. Feuillet, H. Mariette, and N. T. Pelekanos, Phys. Status Solidi B **224**, 13 (2001).

[21] J. Feldmann, G. Peter, E. O. Golbel, P. Dawson, K. Moore, C. Foxon, and R. J. Elliot, Phys. Rev. Lett. **59**, 2337 (1987).

[22] L. C. Andreani, F. Tassone, and F. Bassani, Solid State Commun. **77**, 641 (1991).

[23] D. S. Citrin, Phys. Rev. Lett. **69**, 3353 (1992).

[24] M. Colocci, M. Gurioli, and J. Martinez-Pastor, J. Phys. IV **3**, 3 (1993).

[25] S. Fafard, S. Raymond, G. Wang, R. Leon, D. Leonard, S. Charboneau, J. L. Merz, P. M. Petroff, and J. E. Bowers, Surf. Sci. **361/362**, 778 (1996).